



ELSEVIER

Contents lists available at ScienceDirect

MethodsX

journal homepage: [www.elsevier.com/locate/mex](http://www.elsevier.com/locate/mex)

## Method Article

# Multipurpose setup used to characterize tribo-electrical properties of electrical contact materials



Bruno Alderete<sup>a,\*</sup>, Rafael Puyol<sup>b</sup>, Sebastian Slawik<sup>a</sup>, Eric Espin<sup>a</sup>,  
Frank Mücklich<sup>a</sup>, Sebastian Suarez<sup>a</sup>

<sup>a</sup>Chair of Functional Materials, Saarland University, Campus D3.3, Saarbrücken 66123, Germany

<sup>b</sup>ELEN, ICTEAM, UCLouvain, Place du Levant, 3 bte L5.03.02, Louvain-la-Neuve 1348, Belgium

## A B S T R A C T

Electrical contacts are pervasively found on countless modern devices and systems. It is imperative that connecting components present adequate electrical, mechanical, and chemical characteristics to fulfill the crucial role that they play in the system. To develop an electrical contact material that is tailored for a specific application, different approaches are pursued (e.g., coatings, reinforced composites, alloyed metals, duplex systems, etc.). The manufacturing of electrical contact materials demand a thorough characterization of their electrical properties, mechanical properties, and their resistance to wear, as well as their resistance to atmospheric conditions. Accordingly, commissioning of a novel setup enables a more comprehensive study of the materials that are developed. Therefore, a complete understanding of the material's electrical and tribological characteristics are attained, allowing the production of a material that is compliant with the particular demands of the application for which it is intended. This multipurpose setup was built with higher precision stages and higher accuracy 3-axis force sensor, thus providing the following improvement over the preceding setup:

- Elevated load-bearing capacity (double), higher precision and stability.
- Tribo-electrical characterization (implementation of scratch and fretting tests).
- Environmental control (climate and external vibration).

© 2021 The Authors. Published by Elsevier B.V.

This is an open access article under the CC BY-NC-ND license  
(<http://creativecommons.org/licenses/by-nc-nd/4.0/>)

## A R T I C L E I N F O

*Method name:* Constant current method for automatic electrical contact resistance measurements

*Keywords:* Electrical contact resistance (ECR), Scratch test, Fretting test

*Article history:* Received 5 May 2021; Accepted 23 August 2021; Available online 24 August 2021

\* Corresponding author.

E-mail address: [bruno.alderete@uni-saarland.de](mailto:bruno.alderete@uni-saarland.de) (B. Alderete).

## Specifications table

Subject Area:	Materials Science
More specific subject area:	Tribo-electrical characterization, Carbon-based metal reinforcement and coatings
Method name:	Constant current method for automatic electrical contact resistance measurements
Name and reference of original method:	R. Puyol and S. Suárez, "A contact resistance measurement setup for the study of novel contacts", <i>IEEE URUCON, Montevideo, 2017</i> , pp. 1-4. doi:10.1109/URUCON.2017.8171881
Resource availability:	<ul style="list-style-type: none"> <li>• <a href="https://www.physikinstrumente.store/eu/l-511.20sd00/">https://www.physikinstrumente.store/eu/l-511.20sd00/</a></li> <li>• <a href="https://www.physikinstrumente.store/eu/l-511.2asd00/">https://www.physikinstrumente.store/eu/l-511.2asd00/</a></li> <li>• <a href="https://www.physikinstrumente.store/eu/c-663.12/?c=7">https://www.physikinstrumente.store/eu/c-663.12/?c=7</a></li> <li>• <a href="https://bit.ly/37ntbWP">https://bit.ly/37ntbWP</a></li> <li>• <a href="https://bit.ly/3ysXWWv">https://bit.ly/3ysXWWv</a></li> <li>• <a href="https://bit.ly/2Vxlv0C">https://bit.ly/2Vxlv0C</a></li> <li>• <a href="https://bit.ly/3xs1nLy">https://bit.ly/3xs1nLy</a></li> <li>• <a href="https://github.com/me-systeme/gsv8pypi">https://github.com/me-systeme/gsv8pypi</a></li> <li>• <a href="https://de.tek.com/keithley-source-measure-units/keithley-smu-2400-standard-series-sourcemeter">https://de.tek.com/keithley-source-measure-units/keithley-smu-2400-standard-series-sourcemeter</a></li> <li>• <a href="https://de.tek.com/keithley-low-level-sensitive-and-specialty-instruments/keithley-nanovoltmeter-model-2182a">https://de.tek.com/keithley-low-level-sensitive-and-specialty-instruments/keithley-nanovoltmeter-model-2182a</a></li> <li>• <a href="https://www.tek.com/keithley-accessories/test-fixtures-manual">https://www.tek.com/keithley-accessories/test-fixtures-manual</a></li> <li>• <a href="https://github.com/royerlab/pipython">https://github.com/royerlab/pipython</a></li> <li>• <a href="https://bit.ly/3rXHmLF">https://bit.ly/3rXHmLF</a></li> <li>• <a href="https://www.opta-gmbh.de/produkte/unterbauten/aktiver-unterbau.php">https://www.opta-gmbh.de/produkte/unterbauten/aktiver-unterbau.php</a></li> <li>• <a href="http://www.github.com/brunoalderete/tribo-electrical_testing_rig.git">www.github.com/brunoalderete/tribo-electrical_testing_rig.git</a></li> </ul>

## Method details

Considering the most important characteristics that an electrical contact material should possess, the one at the forefront is the electrical contact resistance (ECR). Using metals that inherently have a low resistivity (such as silver, gold, copper, etc.) ensures that the energy loss throughout the electric circuit will be low. Therefore, when developing new electrical contact materials, it is crucial to quantify the electrical resistance that these materials pose to the flow of current under the contact situation that they will be subjected to. There are several methods to determine ECR, namely: four terminal sensing, three-wire sensing, and two terminal sensing (ohmmeter) under constant current method or constant voltage [1]. Of these methods, the four-probe method is the most common since it is not influenced by the resistance added by the connections and the wiring. In this study, four terminal sensing under constant current was chosen, due to its simplicity and effectiveness. As the name suggests, a constant DC electrical current is applied on the testing material, while the voltage drop is measured between two terminals. Through this measurement, and knowing the value of the applied current, the resistance is simply obtained by Ohm's law.

An efficient ECR measurement is crucial to obtain a complete understanding of the electrical properties of novel and commercially available electrical contacts. The acquisition of reliable ECR measurements is based on the repeatability and the precision of the equipment used. Therefore, the proper selection of the devices is vital. Accordingly, the customizations implemented to the preceding ECR testing rig focus on four key components: the force sensor, the linear stages, the piezoelectric stage, and the environmental control equipment. The selected force sensor not only broadens the range of measurement (by doubling the applicable normal load) but is also capable of measuring strain in three directions. Whereas the perpendicularly mounted linear stages enable the user to characterize the tribological behavior of the contact materials (e.g., connectors) by simulating insertion-removal cycles. Moreover, by implementing a piezoelectric stage, in-operation low-amplitude vibrations can be simulated (fretting) [2,3]. Finally, the incorporation of a climate control chamber and an active vibration dampening stage further expand the range of applications that can be simulated with the multipurpose rig. The former allows the manipulation of the ambient temperature and humidity (improving repeatability), whereas the latter mitigates external factors that may affect the measurements. Furthermore, through specific programming sequences, a wide variety of tests can be carried out, thus combining different normal loads, tangential motion, and ECR measurements.

### Previous ECR setup

Determining the ECR of contact materials has been previously reported by Puyol et al., [4–6] where a setup was developed with the primary objective of determining low-level load-dependent ECR. This setup was able to quantify the ECR in the  $\mu\Omega$  range with a measurement error below 10% for loads below 1 N, and below 1% for loads above 1 N. However, this setup is limited by the linear stage. Considering that the sample to be characterized is mounted on the stage, the system exclusively moves in a single direction. Additionally, the maximum applicable load is restricted by the force sensor's limit (10 N). Nonetheless, this device has proven crucial in conducting ECR of novel composite and coated materials, as well as conducting current sweeps with the help of additional equipment and software.

The setup is constituted by three sectors which work together to perform the measurements (motion and force control, electrical components, and software). The first sector consists of a linear stage (Physik Instrumente M-683.2U4, ultrasonic piezo stage, low-level self-locking, minimum incremental motion of 0.3  $\mu\text{m}$ ) and the uniaxial force sensor (ME-Systeme KD-24 $\pm$ 10N, 0.1% accuracy). The former is used to control the motion of the sample towards and away from the counter electrode, whereas the latter is responsible for regulating the normal load that is applied. Independently, the setup is equipped with a current/voltage sourcing unit (Keithley 2400 SMU) and a nanovoltmeter (Keithley 2182a). These two components handle the electrical parameters of the setup. Finally, the software interface is implemented in LabView to control, observe and extract the parameters and information throughout the entire measurement process.

### New multipurpose ECR setup

To expand upon the aforementioned method, and to acquire vital information on the tribo-electrical characteristics of the novel electrical contact materials (as well as commercially available electrical contact materials), it was sought to develop a new testing rig capable of conducting tribological tests, alongside electrical measurements. Consequently, the possibility for tangential motion (relative to the surface of the sample) was required. By incorporating the capability of lateral motion, scratch tests and reciprocating lateral motion cycles can be performed. The former focuses on the deformation/wear process that arises when the connector is used for the first time. Whereas the objective of the latter is to simulate the deformation that occurs under usual connecting-disconnecting cycles in traditional sliding electrical connectors; thus quantifying the degradation of the contact materials and the electrical characteristics after the initial connection-disconnection process. Moreover, the possibility to conduct high-frequency micro-vibrations was implemented by incorporating a piezoelectric stage. Through this device, naturally occurring vibrations inherent to the intended application of the connector are simulated (fretting test). Furthermore, a force sensor with a higher maximum load of 20 N was selected, in addition to the 3-axis sensing capabilities. Therefore, broadening the range of applicable loads of the setup. Finally, climate control was incorporated, by placing the setup within a climate test chamber, which can replicate in-operation conditions (temperature and humidity). To mitigate external factors from affecting the measurements, the rig was mounted on an active vibration dampening stage, which assures that the climate chamber's vibrations and external factors do not alter the ongoing experiments. The components equipped are summarized in [Table 1](#).

The linear stage motors (M1 and M2) are mounted perpendicularly, relative to each other. M1 is responsible for motion perpendicular to the surface of the sample (normal load), whereas M2 moves parallel to the surface of the sample (tangential motion), as shown in [Fig. 1](#). Both stages are controlled via an individual controller (M3). These two controllers are interconnected with one another via a daisy chain connection and communicate with the software via universal serial bus (USB). The stages move on account of a two-phase stepper motor, with a total of 52 mm travel range and a minimum incremental motion of 0.2  $\mu\text{m}$  for M1 and 0.02  $\mu\text{m}$  for M2. The higher precision of M2 is required to obtain a controlled frictional motion. Whereas the precision of M1 may be lower given that its objective is to control the normal load that is applied. M1 and M2 consist of spindle axis with high-level self-locking. Therefore, M1 increases the stability of the contact forces, granting higher

**Table 1**  
Components required.

Use	Instrument	Manufacturer	Model	Precision	Quantity	Code
Motion	High-precision linear stage	PI	L-511.20SD00	0.2 $\mu\text{m}$	1	M1
Motion	High-precision linear stage with encoder	PI	L-511.2ASD00	0.02 $\mu\text{m}$	1	M2
Motion	Stage controller	PI	C-663.12 Mercury Step	-	2	M3
Motion	Piezoelectric stage	PI	P-750	1 nm	1	M4
Motion	Stage controller	PI	E-709.CHG		1	M5
Force	3-Axis force sensor	ME-Systeme	K3D60a $\pm$ 20N	0.1%	1	F1
Force	Amplifier	ME-Systeme	GSV-8 Sub D44HD	-	1	F2
Electric	Current/Voltage source	Keithley	2400 SMU	$\pm(0.066\% + 20 \mu\text{A})$	1	E1
Electric	Nanovoltmeter	Keithley	2182a	$\pm(30 \text{ ppm} + 4 \text{ ppm})$ at 100 mV range	1	E2
Electric	GPIB to USB adapter	Keithley	KUSB-488b	-	1	E3
Climate	Climate control chamber (temperature and relative humidity)	Vötsch Technik	LabEvent L C/150+10/5	$\pm(0.3\text{-}0.5 \text{ K})$ $\pm(1\text{-}3\% \text{ r.h})$ When controlling temperature and humidity	1	C1
Vibration	Active vibration dampening table	Opta	DMT 600	-	1	V1

force control precision compared to the previous setup's linear stage. The piezoelectric stage (M4) was mounted over the stages and connected to its controller (M5) via a Sub-D special socket 7W2. M5 communicates with the software via USB. M4 has a load capacity of 100 N, with 1 nm vertical accuracy, a maximum travel range of 75  $\mu\text{m}$ , and a maximum frequency of 100 Hz.

The force sensor (F1) was mounted on a stationary column. It is connected to an amplifier (F2) which enhances the electrical signal from the force sensor and communicates it via USB to the software. The force sensor may operate at a maximum force of  $\pm 20 \text{ N}$  (compressive and tensile stress) with an accuracy class of 0.1%. Although F1 and the force sensor from the preceding setup present the same accuracy class (0.1%), a high-accuracy factory calibration was selected, which guarantees measurement repeatability. Moreover, the 3-axis sensing capacity further improves the precision of F1 on account that when loading the device on more than one direction its precision is generally reduced, which is not the case in this force sensor. Regarding F2, the noise level is approximately 10 times lower than the amplifier used in the preceding setup. In other words, with F2 one more decimal number is reliably represented in the F1's measurement. The frequency at which F1 records a measurement can be varied. For force control, the frequency was set at 10 measurements per second. This frequency was chosen since it provides the most precise measurements (precision is load and frequency dependent), granting more precision in the force control. When acquiring the coefficient of friction (CoF), the measurement frequency was set at 100 Hz on account of dynamic process (scratch tests generally do not last for more than a few seconds). Therefore, a tradeoff between higher precision and a larger data pool was chosen.

The electric components are the same as described by Puyol et al. [4], current/voltage source (E1) and nanovoltmeter (E2). E1 is capable of sourcing current from 1 nA to 1.05 A, and voltage from 200  $\mu\text{V}$  to 210 V from its rear control panel terminals. E2 may be programmed with five different measurement ranges from its front control panel terminal: 10 mV, 100 mV, 1 V, 10 V, and 100 V. E1 and E2 are connected to the computer independently via USB using a general purpose interface

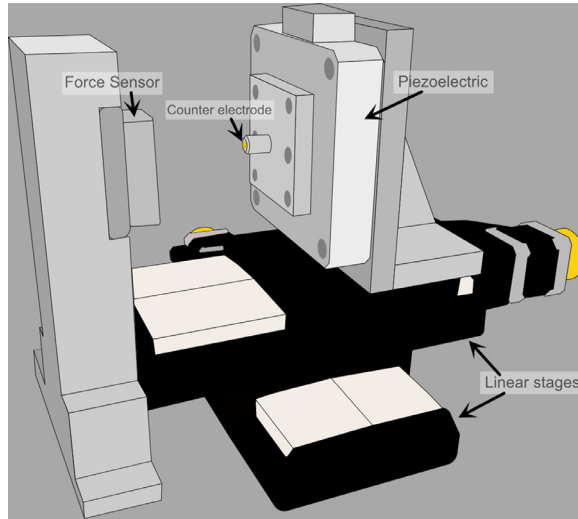
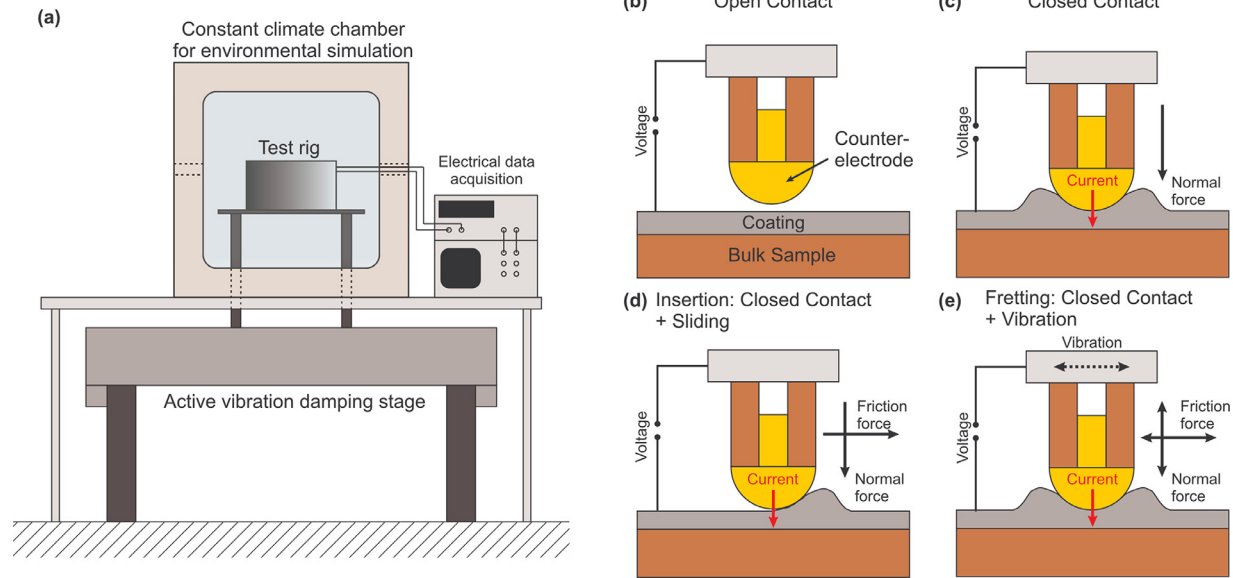


Fig. 1. Schematic representation of novel setup.

bus (GPIB) adapter (E3). An illustration of the setup and possible tests are shown in Fig. 2, whereas Fig. 3 shows a schematic representation of the setup connections. As illustrated in the latter, E1 and E2 have their respective positive terminals connected directly on the sample, whereas their negative terminals are connected on the counter electrode. The location of the positive and negative terminals is not of significance as long the same-sign terminals are connected on the same component. This is due to the fact that the absolute value of the resistance is recorded. To prevent introducing error in the measurements due to thermoelectric effects in the sample and/or conductors, E2 is configured to operate under current reversal mode.

To have a precise control over the atmospheric conditions during the tribo-electrical measurements, the setup is placed in a climate control chamber (LabEvent L C/150+10/5, Vötsch Technik). The chamber is equipped with a thermocouple and a wet bulb humidity sensor to measure the temperature and humidity while in operation, respectively. The thermocouple can be repositioned inside the climate chamber, allowing for a more precise temperature control while running experiments. C1 is able to control temperature between the ranges of 10 and 95°C  $\pm$ (0.3–0.5 K) and relative humidity between 10 and 90%  $\pm$ (1–3% r.h). The error for both parameters is based on an operation state where both are controlled simultaneously. Furthermore, the setup was mounted on an active vibration dampening stage (DMT 600, Opta GmbH) to mitigate the effects of external vibrations while operating. It is highlighted that both components (C1 and V1) are decoupled, thus the vibrations from C1 do not affect the ongoing experiments. The preceding setup does not account with atmospheric control or vibration dampening systems.

The sample is mounted directly on F1, whereas the counter electrode is mounted on M4. Therefore, an insulating Teflon platelet was placed between the counter electrode (where the negative terminals are connected) and M4. Similarly, a Teflon disk – in accordance with the specifications of the manufacturer – was placed between F1 and the sample (where the positive terminals are connected). A sample holder was designed, which was directly mounted on the Teflon disk. Consequently, depending on the weight of the sample holder and sample, the maximum range of F1 is slightly reduced. However, the reduction in maximum load capacity is negligible, below 1% of F1's capacity. The setup was configured in this manner to obtain better accuracy in the fretting tests. Considering that the maximum amplitude of M4 is 75  $\mu$ m, the heavier weight of the sample holder-sample system would reduce the accuracy of the motion.



**Fig. 2.** Schematic representation of a) testing rig inside the climate test chamber and vibration dampening stage; b) open contact between sample and counter electrode; c) ECR measurement; d) ECR and scratch test; e) ECR and fretting test.

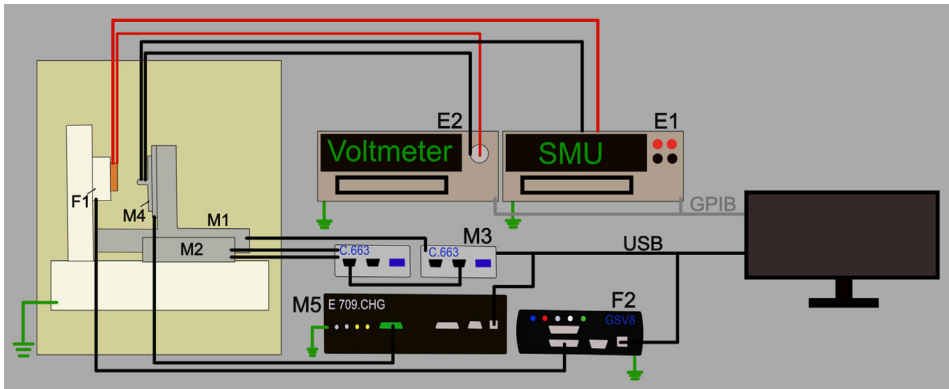


Fig. 3. Schematic representation of the component connections.

### Programming and software

The programming for remote control of the setup was done exclusively in Python 3.8 on Windows OS. Through Python, different motion and reading sequences can be ordered. Certain packages must be installed beforehand, which are external to the original Python installation. Therefore, a virtual environment was created where all the necessary packages were installed. Two specific packages are provided by the manufacturer of the equipment (ME-Systeme and Physik Instrumente). In order to communicate with the motion stage controllers (M3 & M5), GCSDevice package were installed in the directory location where the scripts are saved. This package can be found in GitHub [7]. With this library wrapper, general command set (GCS) is used within Python to send commands to the positioner stages, as well as acquiring information (e.g., current position, movement speed, etc.) [8,9]. Likewise, communication between F1, F2 and Python requires several libraries that are specific for F2 [10]. For E1 and E2, no manufacturer-specific packages were available. However, the instruments support communication via different backend providers, of which different alternatives were scrutinized (e.g., NI-VISA, Keysight IO Libraries, and Pyvisa), opting for the latter. Using Pyvisa, communication between the software and E1 and E2 can be implemented using standard commands for programmable instruments (SCPI) [11,12]. Furthermore, packages such as pandas (to save the data), threading (to run multiple processes simultaneously), and time/datetime were imported. Once the initialization of the components, basic motions and data acquisition have been programmed, different test sequences can be programmed. The fact that different tests and test sequences can be programmed - tailored to the demands of the material that will be analyzed - is an advantage that this setup presents. The following table (Table 2) compiles the scripts and provides a brief summary of their capabilities. These scripts run independently and autonomously. After the user inputs the parameters, they do not require supervision. As an added advantage security steps were added to ensure the safety of the devices. An emergency stop button was installed in case manual power shut off is required. The data acquired by the programs (i.e., measurements taken) and the input parameters are recorded as comma separated values (csv files). All scripts are available in GitHub.

### Method validation

The ECR of tin plated copper samples (Sn/Cu) was analyzed using both testing rigs. The objective was to validate the measurements acquired with the new rig compared to the previous setup. No commercially available devices were found that could be used to validate the results obtained. Therefore, considering the proposed improvements on the self-built previous setup, it was of interest to compare the results obtained with both rigs. Three different loading cycles were evaluated: low loads (0.25, 0.5, 0.75, 1 N), medium loads (1, 2.5, 5, 7.5, 10 N), and high loads (1, 5, 10, 15 N). The

**Table 2**

Obtained data and varying and fixed parameters of different Python scripts.

Program	Script name	Description
1	current_sweep.py	Takes ECR measurement by varying the applied current. E2 range and number of ECR measurements can be varied. The user can input the currents.
2	ecr.py	Takes ECR measurements by varying the normal load. The current, measurements per load, and E2 range can be varied. The user can input the loads desired.
3	scratch_ecr.py	Carries out a scratch test, followed by ECR measurements. The scratch load (and ECR load), and track length are set by the user. E2 range and number of ECR measurements can be varied. CoF and ECR are acquired.
4	fretting_ecr.py	Carries out fretting test, followed by ECR measurements. The fretting load, number of cycles, and amplitude are set by the user. E2 range and number of ECR measurements can be varied. ECR is acquired.
5	scratch_fretting.py	Carries out scratch test, followed by fretting. The user input and varying parameters are the same as program 3 and 4. CoF is acquired.
6	connection_ecr_disconnection.py	Simulates connection and disconnection cycles. A scratch test is performed, followed by ECR measurements and a scratch test returning to the starting position. The number of cycles, normal load, and scratch track are user input. E2 range and number of ECR measurements can be varied. CoF in both directions and ECR are acquired.

latter, however, was only measured using the new setup given the extended load ranges. Furthermore, the range of E2 was set at 0.1 V for medium and high loads, whereas it was set at 1 V for low loads to prevent the equipment from overflowing. It is important to highlight that the rig is not capable of changing the voltmeter's range within a single measurement cycle. The range can only be changed manually when the program starts. In this case, two different ranges were used to showcase the optimal accuracy of E2. As in many characterization techniques, one should have a previous idea about the order of magnitude of the variable that will be determined. It is known that low load measurements would grant higher ECR values than medium or high loads. Therefore, to prevent E2 from overflowing, a higher voltage range was selected. In actual measurements, where comparability between different measurement cycles is important, only one voltage range should be used. In all cycles, the current was set at 100 mA, so as to avoid any microstructural changes in the metallic sample (dry circuit testing) [13]. For each force, five measurements were taken and averaged, the results obtained are shown in Fig. 4. Observing Fig. 4 a, the ECR measurements for both setups are similar. The initial resistance at 0.25 N is slightly higher for the traditional setup. However, for 1 N the resistance is lower compared to the new setup. Despite some differences, the error for both systems are relatively low, and the ECR values follow the same tendency. Given the low contacting loads, the ECR values are relatively high, in the 1  $\Omega$  range. As Fig. 4 b depicts, similar tendencies are observed in both setups for medium load range. The initial ECR in the previous setup is significantly higher than in the proposed setup; however, the ECR sharply decreases for the second force. Similarly, the error observed in the new setup is elevated in the first two measurements (between 50 and 70 m $\Omega$ ). However, for higher applied loads the error is reduced to below 10 m $\Omega$  (representing between 0.5% and 8% error of the current measurements). For higher normal loads the error observed decreases. ECR measurements for high normal loads, carried out with the proposed setup, are shown in Fig. 4 c. As observed, the error for the lower half of the measurements is relatively high, but is reduced for elevated normal loads. The tendency of this curve is similar to the one observed for medium normal loads, recording lower ECR throughout the cycles. The minimum ECR value recorded for 15, 10 and 5 N (in the unloading semi-cycle) are approximately 20 m $\Omega$ .

Additionally, ECR measurements were carried out at a constant normal load of 2 N varying the current in the following sequence: 30  $\mu$ A, 0.1 mA, 0.3 mA, 1 mA, 3 mA, 10 mA, 100 mA, 300 mA, and 1

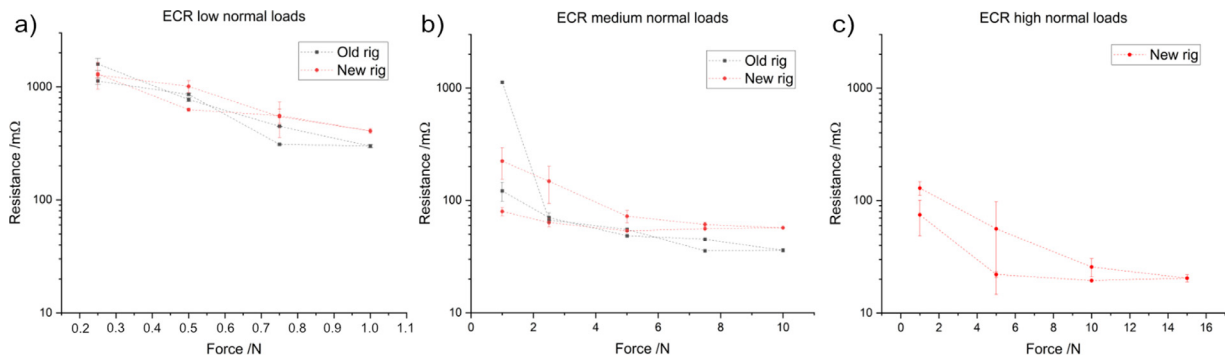


**Fig. 4.** ECR for a) low normal load range; b) medium normal load range; c) high normal load range.

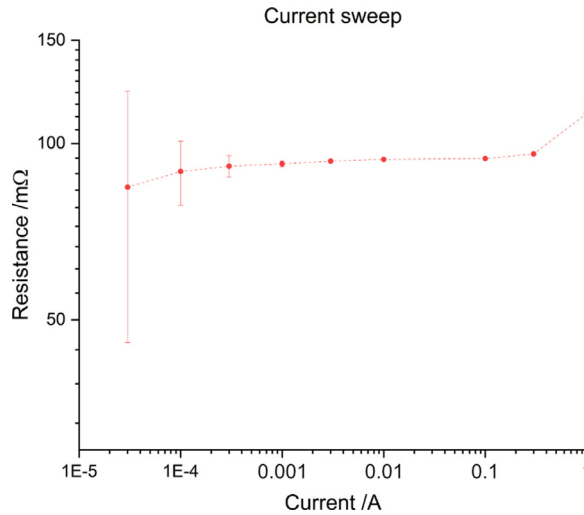


Fig. 5. ECR at constant normal load (2 N), varying current from 30  $\mu$ A – 1 A.

A. Five ECR measurements were taken for each current. The average ECR appears constant throughout the sweep, as shown in Fig. 5. Given the low current used (30  $\mu$ A and 0.1 mA), and the elevated range used in E2 (1 V), the error for these two measurements is more significant compared to measurements carried out at higher currents. This range was selected due to the fact that E2 would overflow if 100 mV range was used.

Additionally, scratch and fretting tests were conducted on Sn/Cu samples using the proposed setup. Scanning electron microscopy (SEM) micrographs using backscattered electron detector (BSE) of the scratch track and fretting mark are shown in Fig. 6. The scratch test was carried out at a normal load of 5 N for a total length of 10 mm with a sliding speed of 15 mm/s. Whereas the fretting test was carried out with an amplitude of 75  $\mu$ m, a frequency of 9 Hz for 100 cycles. The rig was programmed in a way in which the normal load is actively compensated only during fretting tests. That is a consequence of the force sensor's data collection rate. During a scratch test, the force sensor constantly collects the registered force in the tangential and normal axis; this information is later used to determine the CoF. However, due to the short duration of the scratch test (generally below 1.5 s), the test does not last long enough for a proper normal load compensation. Therefore, to resolve this issue, an appropriate sample holder was designed (for each specific type of sample that will be measured). With this sample holder, one can ensure that the surface of the sample is perpendicular to the counter electrode at all times. During fretting, ECR, and indentations this problem does not arise since the CoF is not recorded. Therefore, the force sensor is used exclusively for normal load control.

#### Accuracy and uncertainty analysis

The resistance measurement was made using the traditional Kelvin method. The current was sourced by E1 and the voltage was measured with E2. Equipment manufacturers usually provide the uncertainty in the sourcing or measuring mode expressed by an uncertainty in the measurements, plus an uncertainty in the range. This numeric value is complemented by two more coefficients, which are expressed in the same way. That must be multiplied by the temperature exceedance from the permissible range to compensate for temperature effects [14]. Both E1 and E2 require temperature correction when working below 18°C or above 28°C. However, for this study, the temperature was kept between these ranges. Therefore, the correction factor was not required. The coefficients usually drift as time from calibration progresses. As a preventive measure the worst-case values were

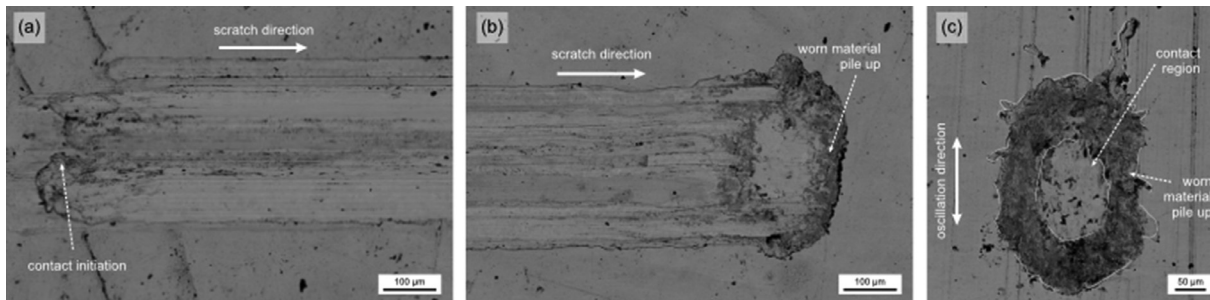


**Fig. 6.** SEM micrograph of a) beginning of scratch track; b) ending of scratch track; c) fretting mark.

**Table 3**

Calculated resistance standard deviation for different voltage ranges.

Keithley 2400 SMU range	Keithley 2128a range	$\sigma$
100 $\mu$ A	10 mV	171.3 n $\Omega$
100 $\mu$ A	100 mV	170.6 n $\Omega$
100 $\mu$ A	1 V	170.4 n $\Omega$

used. Consequently, a coefficient corresponding to a calibration of more than two years before the experiment was adopted.

Alternatively, the data (sourced or measured) can be interpreted as a random variable. The mean of the random variable is the value of the physical process we want to obtain, whereas the variance is composed by the addition of the range and measured uncertainty. Therefore, the variance is a function of the mean. Therefore, once the mean is set, the distribution is obtained. Furthermore, it was assumed that the uncertainty provided by the manufacturers corresponds to 3-sigmas. In other words, the measurements will fall within the uncertainty ranges provided 99.73% of the times.

To determine the resistance, two normally distributed random variables must be divided. However, this division yields another random variable with no finite moments and several different distributions, depending on the parameters. Nonetheless, several authors have proposed ways of approximating the distribution with a normal one and have also studied the conditions that make this approximation valid [15]. Therefore, the mean and standard deviation for the measured resistance can be determined from those of the voltage and current values through the following equations (Eq. 1 and Eq. 2):

$$\mu_R = \frac{\mu_V}{\mu_I} \quad (1)$$

$$\sigma_R = \mu_R \sqrt{\left( \frac{\sigma_V^2}{\mu_V^2} + \frac{\sigma_I^2}{\mu_I^2} \right)} \quad (2)$$

Kueth et al. [16] has stipulated a condition that is sufficient for approximating the distribution of the resistance as a normal distribution. This condition is shown on Eq. 3. In this case, the condition is not difficult to satisfy, although for other applications it can be harder. Therefore, several authors have proposed alternative methods [17,18]. The mean and standard deviations for the optimal equipment ranges are shown in Table 3. It can be observed that all values satisfy the condition proposed by Kueth et al.

$$\frac{\sigma_I}{\mu_I} \leq 0.1 \quad (3)$$

Both electrical devices have several ranges, many combinations of these provide suitable ranges for performing the measurements. Using the aforementioned equations, one can determine the range that minimizes uncertainty. Although several voltage ranges fall within the measurement range for a single current, the best choice is to use the largest current that is allowed by the voltage range (without overflowing). The part of the uncertainty related to the reading will be constant, but the fixed part related to the range will have a smaller impact if the measurand is closer to the upper limit of the range. Given the materials that will be analyzed with these setups, it is expected that the resistance will be in the range of 1 m $\Omega$ . Therefore, the uncertainty for all the combinations of voltage and current ranges when measuring 1 m $\Omega$  using the largest possible current per range is shown in Fig. 7. As the arrow indicates, there are three possible configurations with almost identical uncertainty levels, shown in Table 3, of which the latter range offers the lowest standard deviation. Furthermore, the lowest resistance can be measured using the 10 mV range, whereas the highest resistance can be measured with the 1 V range. Regarding the 100 mV range, it is the best choice when it is expected that the resistance will fluctuate in both directions.

Finally, the error present in the proposed setup while the stages control the normal load to the set value is shown in Fig. 8. For this plot, between 100 and 200 normal load measurements were

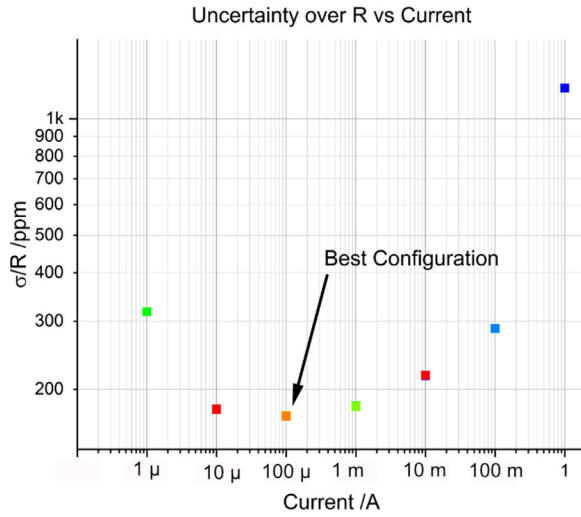


Fig. 7. Uncertainty on the measurements vs. current for the different configurations.

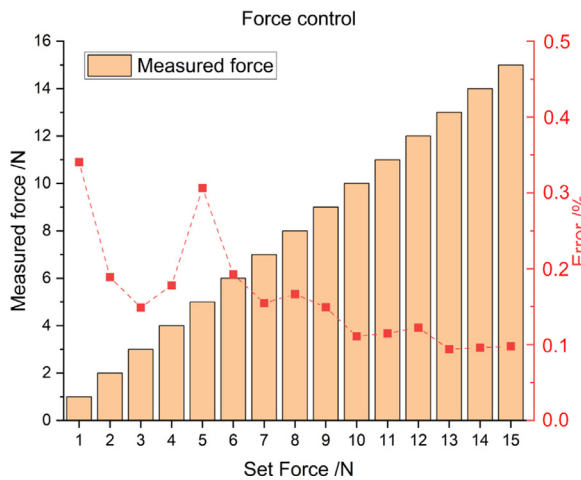


Fig. 8. Error while controlling normal load.

recorded while the stages controlled said force. As the graph depicts, the error never surpassed 0.35%, with values as low as 0.10% for higher normal loads.

*Concluding remarks*

This method article presents the added possibilities of a new multipurpose setup compared to the preceding. By implementing the additional motor stages and using a force sensor with a higher permissible load, the capabilities are extended; thus, achieving more in-depth information on the tribo-electrical characteristics of electrical contact materials. Additionally, the higher precision of the linear stages (along with the lower minimum incremental motion) allows a finer control of applied normal loads and precise lateral motions. The incorporation of the piezoelectric stage allows micro-oscillations that simulate in-operation fretting wear. As demonstrated in the method validation, the

ECR curves for the same force range are similar in magnitude when measured with both rigs; proving that the new setup effectively provides the resistance measurement. Moreover, the selection of high-precision linear stages and high-accuracy 3D force sensor is reflected upon the accuracy and uncertainty analysis. Therefore, rendering considerably precise measurements (regarding applied normal load, measurement of tangential load, and electrical measurements) with an offset from the set force as low as 0.1%. Furthermore, the atmospheric control chamber and active vibration dampening stage produce more reproducible measurements, avoiding the influence of uncontrollable external factors on the measurements. The scripts developed and programming sequences were written in Python, all of which are open-source and available in GitHub.

## Acknowledgement

B.A. wishes to acknowledge the support from the German Academic Exchange Service (DAAD). We acknowledge support by the Deutsche Forschungsgemeinschaft (DFG, German Research Foundation) and Saarland University within the funding program Open Access Publishing. The TÜV Saarland Stiftung is gratefully acknowledged for financially supporting the project. The authors gratefully acknowledge funding in the ZuMat project, supported by the State of Saarland from the European Regional Development Fund (Europäischen Fonds für Regionale Entwicklung, EFRE).

## Declaration of Competing Interest

The authors declare that they have no known competing financial interests or personal relationships that could have appeared to influence the work reported in this paper.

## References

- [1] G.T. Meaden, *Electrical Resistance of Metals*, Springer US, 2013, doi:[10.1007/978-1-4899-5717-7](https://doi.org/10.1007/978-1-4899-5717-7).
- [2] A. Bouzera, E. Carvou, N. Ben Jemaa, R. El Abdi, L. Tristani, E.M. Zindine, Minimum fretting amplitude in medium force for connector coated material and pure metals, in: *Electr. Contacts, Proc. Annu. Holm Conf. Electr. Contacts*, 2010, pp. 101–107, doi:[10.1109/HOLM.2010.5619557](https://doi.org/10.1109/HOLM.2010.5619557).
- [3] D. Gagnon, M. Braunovic, J. Masounave, Effect of fretting slip amplitude on the friction behaviour of electrical contact materials, in: *Electr. Contacts, Proc. Annu. Holm Conf. Electr. Contacts*, 2005, pp. 186–195, doi:[10.1109/HOLM.2005.1518243](https://doi.org/10.1109/HOLM.2005.1518243), vol. 2005.
- [4] R. Puyol, S. Suarez, A Contact Resistance Measurement Setup for the Study of Novel Contacts, *IEEE URUCON (2017) 1–4*, doi:[10.1109/URUCON.2017.8171881](https://doi.org/10.1109/URUCON.2017.8171881).
- [5] K.E. Trinh, F. Mücklich, E. Ramos-Moore, The role of microstructure and surface topography in the electrical behavior of Sn-coated Cu contacts, in: *27th Int. Conf. Electr. Contacts, ICEC 2014 - Proc*, 2014, pp. 243–248.
- [6] K.E. Trinh, E. Ramos-Moore, I. Green, C. Pauly, M. Zamanzade, F. Mücklich, Topographical and Microstructural Effects of Laser Surface Texturing on Tin-Coated Copper Electrical Connectors under Load Cycling, *IEEE Trans. Components, Packag. Manuf. Technol.* 7 (4) (2017) 582–590, doi:[10.1109/TCPMT.2017.2659224](https://doi.org/10.1109/TCPMT.2017.2659224).
- [7] Royerlab, “GCSDevice.” [www.github.com/royerlab/pipython](https://www.github.com/royerlab/pipython) (accessed Dec. 07, 2020).
- [8] Physik Instrumente, in: *C-663 Mercury Step Stepper Motor Controller User Manual*, PI, Karlsruhe, 2020, p. 295.
- [9] Physik Instrumente, in: *PZ222E User Manual E-709 Digital Piezo Controller, 1 Channel, -30 to 130 V, PI*, Karlsruhe, 2019, p. 269.
- [10] ME-Systeme, “GSV8-Py.” [www.github.com/me-systeme/gsv8pypi](https://www.github.com/me-systeme/gsv8pypi) (accessed Nov. 14, 2020).
- [11] K. Instruments, Keithley 2400 User’s manual, Cleveland (2011) [Online]. Available [www.tek.com/keithley-source-measure-units/keithley-smu-2400-series-source-meter-manual/series-2400-source-meter](http://www.tek.com/keithley-source-measure-units/keithley-smu-2400-series-source-meter-manual/series-2400-source-meter).
- [12] K. Instruments, Model 2182/2182A Nanovoltmeter User’s Manual, Cleveland (2004) [Online]. Available: [www.tek.com/product-support?series=Keithley Nanovoltmeter Model 2182A%0A](http://www.tek.com/product-support?series=Keithley%20Nanovoltmeter%20Model%202182A%20A).
- [13] E.M. Bock, Low-Level Contact Resistance Characterization, *AMP J. Technol.* 3 (1993) 64–68.
- [14] Tektronix *Low Level Measurements Handbook*, Precision DC Current, Voltage and Resistance Measurements, 7th Editio, 2016 Beaverton.
- [15] E. Díaz-Francés, F.J. Rubio, On the existence of a normal approximation to the distribution of the ratio of two independent normal random variables, *Stat. Pap.* 54 (2) (2013) 309–323, doi:[10.1007/s00362-012-0429-2](https://doi.org/10.1007/s00362-012-0429-2).
- [16] D.O. Kuethe, A. Caprihan, H.M. Gach, I.J. Lowe, E. Fukushima, *Imaging Obstructed Ventilation with NMR using Inert Fluorinated Gases*, *J. Appl. Physiol.* 88 (2000) 2279–2286.
- [17] G. Marsaglia, Ratios of Normal Variables and Ratios of Sums of Uniform Variables, *J. Am. Stat. Assoc.* 60 (309) (1965) 193–204, doi:[10.1080/01621459.1965.10480783](https://doi.org/10.1080/01621459.1965.10480783).
- [18] J. Hayya, D. Armstrong, N. Gressis, A Note on the Ratio of Two Normally Distributed Variables, *Manage. Sci.* 21 (11) (1975) 1338–1341, doi:[10.1287/mnsc.21.11.1338](https://doi.org/10.1287/mnsc.21.11.1338).